Two-Dimensional Analysis of a Flow in an MPD Thruster

By

Hiroyuki YAMADA*, Takashi AO* and Toshi FUJIWARA*

(January 10, 1985)

1. INTRODUCTION

The MPD thruster is promising as a future propulsion system from the viewpoint of high specific impulse, simplicity of control, capability of low voltage drive etc. Despite these fundamental advantages, it is difficult in actual experiments to maintain uniform current distribution, and, in addition, various abnormal phenomena happen. The MPD thrusters are still poorly understood, because the conprehensive measurements of the complicated flow and electromagnetic fields have not been performed.

The present study deals with the numerical simulation of a magneto-hydrodynamic two-dimensional flow based on the one-fluid model, using a second-order-accurate difference scheme. The thruster is composed of a hollow cylindrical anode and a cone-cylinder-shaped cathode. The calculated domain is also enlarged in comparison with the previous analysis [*3*], attempting this simulation to reproduce actual phenomena observed in experiments.

2. FORMULATION AND METHOD OF ANALYSIS

To start with, it is noted that the following assumptions are applied to the present analysis:

1) The flow and electromagnetic fields are axi-symmetric.
2) The fluid is continuous, isotropic and macroscopically neutral. Microscopic phenomena, e.g., the electrode sheath or starvation, are ignored.
3) No ionization processes, chemical reactions and heat of reaction are considered. Therefore the gas is singly ionized already at inlet, where the simulation starts.
4) The fluid is regarded as an ideal gas in thermal equilibrium. Here the working fluid is Argon.
5) All the magnetic field is self-induced and therefore has azimuthal component only.
6) No transport phenomena other than electric and magnetic conductions are considered.
7) The generalized Ohm law holds between electric field and current density, taking account of the Hall effect. However, the displacement current term of the Maxwell equation is regarded as negligibly small.

* Department of Aeronautical Engineering, Nagoya University

8) The velocity and pressure at the inlet, the downstream pressure and the total current are specified.

The thruster geometry, the coordinate system and the calculated physical domain are shown in Fig. 1. This analysis handles a case where the cathode tip is of cone shape, corresponding to the existing experiments. The fundamental equations governing the gas motion are written in a non-dimensional form as follows:

Continuity Eq.;

$$\frac{\partial \hat{\rho}}{\partial \hat{t}}+\frac{1}{\hat{r}}\frac{\partial}{\partial \hat{r}}(\hat{\rho}\hat{u}\hat{r})+\frac{\partial}{\partial \hat{z}}(\hat{\rho}\hat{v})=0, \tag{1}$$

Momentum Eqs.;

$$\frac{\partial}{\partial \hat{t}}(\hat{\rho}\hat{u})+\frac{1}{\hat{r}}\frac{\partial}{\partial \hat{r}}(\hat{\rho}\hat{u}^2\hat{r})+\frac{\partial \hat{p}}{\partial \hat{r}}+\frac{\partial}{\partial \hat{z}}(\hat{\rho}\hat{u}\hat{v})=-\hat{j}_z\hat{B}, \tag{2}$$

$$\frac{\partial}{\partial \hat{t}}(\hat{\rho}\hat{v})+\frac{1}{\hat{r}}\frac{\partial}{\partial \hat{r}}(\hat{\rho}\hat{u}\hat{v}\hat{r})+\frac{\partial}{\partial \hat{z}}(\hat{\rho}\hat{v}+\hat{p})=\hat{j}_r\hat{B}, \tag{3}$$

Energy Eq.;

$$\frac{\partial \hat{q}}{\partial \hat{t}}+\frac{1}{\hat{r}}\frac{\partial}{\partial \hat{r}}(\hat{q}_r\hat{r})+\frac{\partial}{\partial \hat{z}}(\boldsymbol{q}_z)=0, \tag{4}$$

$$\hat{q}=\frac{1}{2}\hat{e}|\hat{\boldsymbol{V}}|^2+\frac{1}{\gamma-1}\hat{\rho}\hat{T}+\hat{B}^2, \tag{5}$$

$$\boldsymbol{q}=(p+q)\boldsymbol{V}+2\boldsymbol{E}\times\boldsymbol{B}, \tag{6}$$

Maxwell Eqs.;

$$\frac{\partial \hat{B}}{\partial \hat{t}}=\frac{\partial \hat{E}_z}{\partial \hat{r}}-\frac{\partial \hat{E}_r}{\partial \hat{z}}, \tag{7}$$

$$\hat{j}_r=-2\frac{\partial \hat{B}}{\partial \hat{z}}, \qquad \hat{j}_z=\frac{2}{\hat{r}}\frac{\partial}{\partial \hat{r}}(\hat{r}\hat{B}), \tag{8}$$

Generalized Ohm Law;

$$\begin{pmatrix}\hat{j}_r\\ \hat{j}_z\end{pmatrix}=\frac{2R_m\sigma}{1+he^2}\begin{pmatrix}1 & he\\ -he & 1\end{pmatrix}\begin{pmatrix}\hat{E}_r-\hat{v}\hat{B}\\ \hat{E}_z+\hat{u}\hat{B}\end{pmatrix}, \tag{9}$$

he; Hall parameter.

Eq. of State;

$$\hat{p}=\hat{\rho}\hat{T}, \tag{10}$$

where ˆ signifies the dimensionless values, $\hat{\rho}$ the density, $\hat{V}=(\hat{u}, 0, \hat{v})$ the gas velocity, $\hat{p}$ the pressure, $\hat{T}$ the temperature, $\hat{q}$ the energy density, $\hat{\boldsymbol{q}}=(\hat{q}_r, 0, \hat{q}_z)$ the energy flux, $\hat{\boldsymbol{j}}=(\hat{j}_r,0,\hat{j}_z)$ the current density, $\hat{\boldsymbol{B}}=(0, \hat{B}, 0)$ the magnetic flux density, and $\hat{\boldsymbol{E}}=(\hat{E}_r,0,\hat{E}_z)$ the electric field, respectively.

The physical properties are non-dimensionalized as in the following:

$$\left.\begin{aligned} &\rho=\frac{\dot{m}}{V_m}\hat{\rho}, \quad u=V_m\hat{u}, \quad v=V_m\hat{v}, \quad T=\frac{V_m^2}{R}\hat{T}, \\ &p=P_m\hat{p}, \quad B=B_0\hat{B}, \quad E_{r,z}=V_mB_0\hat{E}_{r,z}, \\ &j_{r,z}=\frac{B_0}{2\mu_0R_c}\hat{j}_{r,z}, \quad \sigma=\sigma_0\hat{\sigma}, \end{aligned}\right\} \tag{11}$$

where R_c represents the cathode radius, V_m the magnetic acoustic speed, P_m the magnetic pressure at the thruster inlet, $\dot{m}$ the mass flow rate per unit area, σ the electric conductivity, B_0 the magnetic flux density on the cathode root surface and μ_0 the permeability, and R the gas constant, respectively.

Here B_0, P_m *and* V_m are expressed by using the total current $J=\int j d\boldsymbol{S}$ and $\dot{m}$.

$$B_0=\frac{\mu_0 J}{2\pi R_c}, \quad P_m=\frac{B_0^2}{2\mu_0}, \quad V_m=\frac{B_0^2}{2\mu_0\dot{m}}. \tag{12}$$

R_m appearing in the generalized Ohm law denotes the magnetic Reynolds number, which can be written as:

$$R_m=\mu_0\sigma_0V_mR_c=\frac{\mu_0^2\sigma_0}{8\pi^2R_c}\left(\frac{J^2}{\dot{m}}\right), \tag{13}$$

where $J^2/\dot{m}$ is a key parameter representing the characteristics of an MPD thruster. When $J^2/\dot{m}$ exceeds a critical value, cathode erosion tends to increase while the spatial distribution of velocity, current, electric field etc. starts being disturbed [*1*]. The electrical conductivity σ is determined using the Spitzer formula for a singly ionized Argon plasma [*2*]:

$$\sigma=1.5\times10^{-3}T^{3/2}, \tag{14}$$

which can be written as:

$$\sigma=(en_e)\mu_e, \tag{15}$$

where e is the quantum of electricity, n_e the number density of electron, and μ_e the mobility, respectively. Therefore, using these properties, the Hall parameter he is written as:

$$he=\mu_e B=\frac{\sigma}{en_e}B=\frac{m_e}{e}\left(\frac{\sigma}{\rho}B\right). \tag{16}$$

where m_e denotes the electron mass.

The boundary conditions are imposed on the magnetic field as follows:

$$\text{At the inlet;}\quad B=-B_0\frac{R_c}{r}. \tag{17}$$

$$\text{On the axis of symmetry;}\quad B=0, \tag{18}$$

$$\text{At the downstream boundary;}\quad B=0. \tag{19}$$

$$(r=2.0\times R_c \text{ or } z=1.5\times L)$$

3. Numerical Analysis

As our numerical difference scheme, the 2nd-order explicit MacCormack method is used in its time-splitting form. The fundamental equations (1)~(7) can be expressed as:

$$\frac{\partial f}{\partial t}\frac{1}{r}\frac{\partial}{\partial r}(rF)+\frac{\partial G}{\partial r}+\frac{\partial H}{\partial z}=0, \tag{20}$$

when cylindrical coordinates are utilized assuming axial symmetry. If we define a time-advancing operator $L(\Delta t)$ by

$$f_{i,j}^{n+1}=L(\Delta t)f_{i,j}^{n}, \tag{21}$$

then $L(\Delta t)$ can be approximated to the 2nd-order accuracy by the two one-dimensional operators $L_r(\Delta t)$ and $L_z(\Delta t)$ defined for the time-split forms of Eq. (20);

$$\frac{\partial f}{\partial t}+\frac{1}{r}\frac{\partial}{\partial r}(rF)+\frac{\partial G}{\partial r}=0, \tag{22}$$

$$\frac{\partial f}{\partial t}+\frac{\partial H}{\partial z}=0, \tag{23}$$

In order words, we have

$$L(\Delta t)=L_z(\Delta t/2)\cdot L_r(\Delta t)\cdot L_z(\Delta t/2), \tag{24}$$

Looking at the geometry shown in Fig. 1 and the electromagnetic field quantities in addition to fluid mechanical variables, it may be a good idea to describe boundary conditions to a certain detailed extent.

In general, grid cells are specified as rectangles located in parallel with the axis of

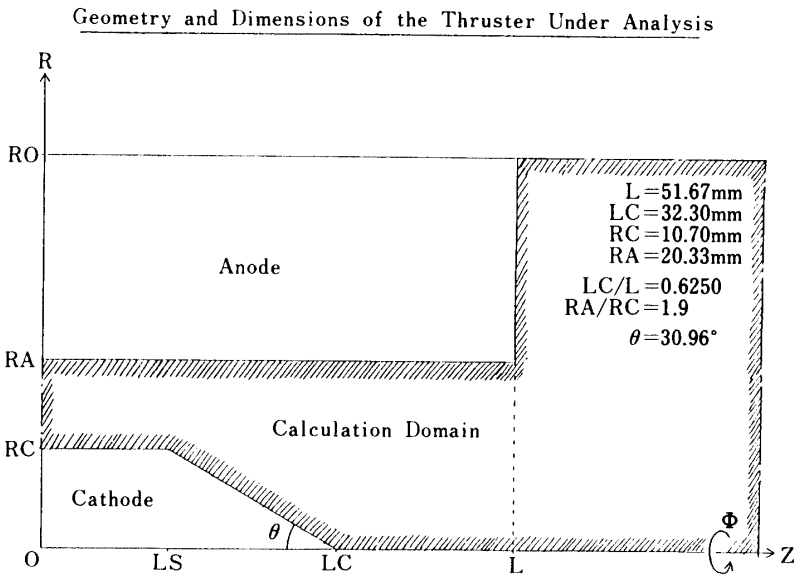

Fig. 1. Thruster geometry and coordinate system.

symmetry.

1) The boundary conditions on the solid surface are imposed as follows:

$$V_n=0, \quad E_t=0, \quad \text{and} \quad \frac{\partial f}{\partial \boldsymbol{n}}=0;\ f=\rho,\ V_t,\ T,\ p,\ E_n,\ B, \tag{25}$$

where the subscript n represents the normal components to the solid surface, t the tangential component and $\boldsymbol{n}$ the outward normal unit vector to the wall. Both on the surface of the anode and on the cylindrical cathode, a grid is set at the point of symmetry across the surface where the principle of reflection is applied.

On the anode inside surface, we have, as shown in Fig. 2(a) and 2(d),

$$\begin{aligned} &f_{i,j+1}=-f_{i,j}, \quad \text{for} \quad f=u,\ E_z, \quad \text{while} \\ &g_{i,j+1}=g_{i,j}, \quad \text{for} \quad g=\rho,\ v,\ T,\ p,\ E_r,\ B. \end{aligned} \tag{26}$$

On the cylindrical cathode surface, we have, as shown in Fig. 2(b),

$$\begin{aligned} &f_{i,j-1}=-f_{i,j}, \quad \text{for} \quad f=u,\ E_z \quad \text{while} \\ &g_{i,j-1}=g_{i,j}, \quad \text{for} \quad g=\rho,\ v,\ T,\ p,\ E_r,\ B. \end{aligned} \tag{27}$$

On the anode vertical surface, we have, as shown in Fig. 2(c),

$$\begin{aligned} &f_{i-1,j}=-f_{i,j}, \quad \text{for} \quad f=v,\ E_r, \quad \text{while} \\ &g_{i-1,j}=g_{i,j}, \quad \text{for} \quad g=\rho,\ u,\ T,\ p,\ E_z,\ B. \end{aligned} \tag{28}$$

2) The conial cathode surface is treated in a complicated manner (see Figs. 2(e) and 2(f)). What is different from 1) is that there is no symmetry, with respect to the boundary, between the two closest points across the surface. Therefore, the property at

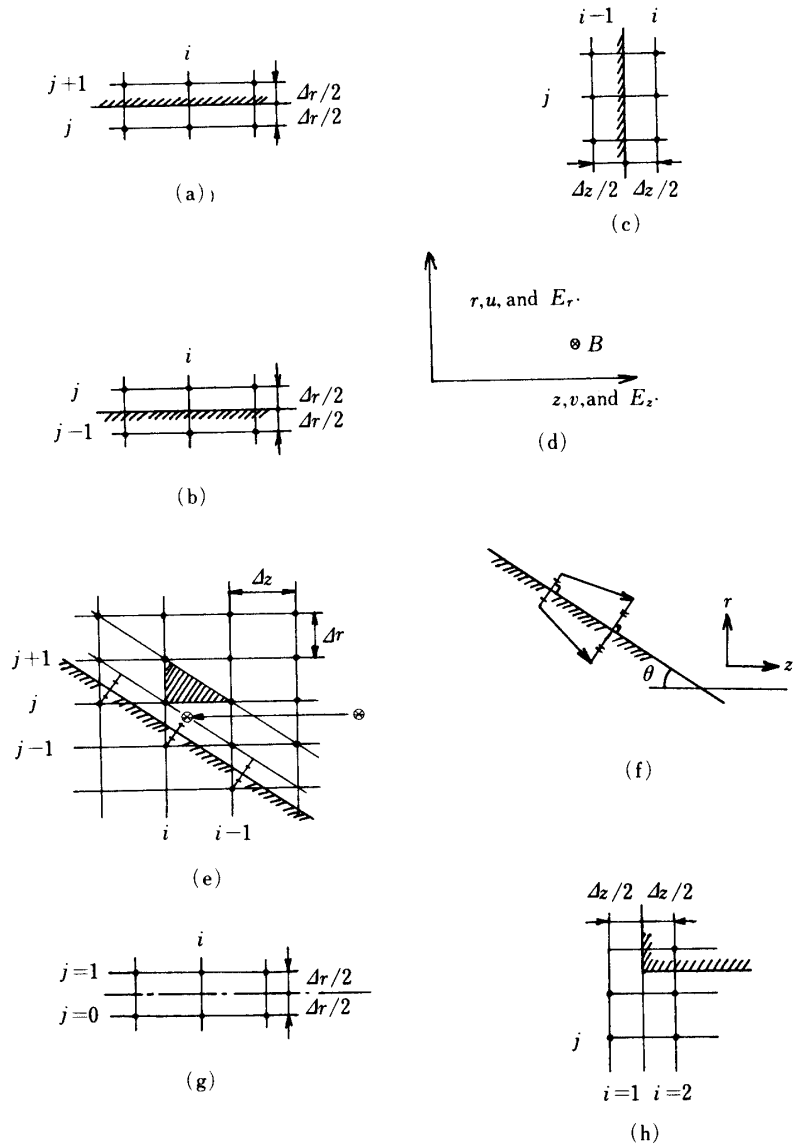

Fig. 2. Boundary mesh configurations.

the inner point symmetrical to an outer grid point is calculated by simple interpolation, as shown in Fig. 2(e):

$$f_{i,j-1}=f_{i,j}+\frac{1}{1+\left(\frac{\Delta z}{\Delta r}\right)^2}(f_{i+1,j}-f_{i,j+1}), \tag{29}$$

where $f=\rho$, u, v, T, p, B, E_r and E_z.

As to vector quantities like velocity and electric field, it is more convenient to use the following transformation (30), as shown in Fig. 2(f):

$$\begin{bmatrix}(f_{i,j-1})_r\\(f_{i,j-1})_z\end{bmatrix}=-\begin{bmatrix}\cos 2\theta & \sin 2\theta\\ \sin 2\theta & -\cos 2\theta\end{bmatrix}\begin{bmatrix}(f^*_{i,j-1})_r\\(f^*_{i,j-1})_z\end{bmatrix}, \tag{30}$$

where $f_r=u$, E_r and $f_z=v$, E_z.

3) The boundary conditions on the axis of symmetry are as follows:

$$\text{At} \quad r=0;\ u=0,\ E=0,\ B=0 \quad \text{and} \quad \frac{1}{r}\frac{\partial f}{\partial r}=0, \tag{31}$$

where $f=\rho$, v, T, p and E_z.

Since the axis has singular characters, the grids are shifted by a half radial mesh size, and then the principle of reflection is applied, as shown in Eqs. (32) and (33) and Fig. 2(g);

$$f_{i,0}=-f_{i,1}, \quad \text{for} \quad f=u,\ E_r,\ B \text{ and } r. \tag{32}$$

$$g_{i,0}=g_{i,1}, \quad \text{for} \quad g=\rho,\ v,\ T,\ p \text{ and } E_z. \tag{33}$$

4) At the inlet of the thruster, each property remains unchanged from its initial value. As indicated in Fig. 2(h), we put

$$\left.\begin{aligned} &f_{1,j}=f_{in}, \quad \text{for} \quad f=\rho,\ v,\ T \text{ and } p, \\ &u_{1,j}=0 \quad \text{and} \quad B_{1,j}=-B_0\frac{R_c}{r_j}. \end{aligned}\right\} \tag{34}$$

5) At the downstream boundary, we have

$$B_{i,j}=0 \quad \text{and} \quad f_{i,j}=f_{i-1,j}.$$

At the upper boundary, we have

$$B_{i,j}=0 \quad \text{and} \quad f_{i,j}=f_{i,j-1}, \quad \text{for} \quad f=\rho,\ u,\ v,\ T \text{ and } p. \tag{35}$$

The downstream and upper boundaries are located at $z=1.5\times L$ and $r=2.0\times R_c$, respectively, where L denotes the thruster length and R_c the cathode radius.

4. Results

In order to provide a reasonable comparison with available experimental observations, the parameters appearing in the present analysis are selected as follows:

$$\left.\begin{aligned} &R_m=1.007, \quad V/V_m=0.028, \quad p/P_m=0.016, \\ &L_c/L=0.625, \quad R_a/R_c=1.9, \quad \Delta r/R_c=0.107, \\ &\Delta z/R_c=0.178. \end{aligned}\right\} \tag{36}$$

where L represents the thruster length, L_c the cathode length, and R_a the anode caliber, respectively.

Time-dependent fields have been solved using the MacCormack second-order explicit

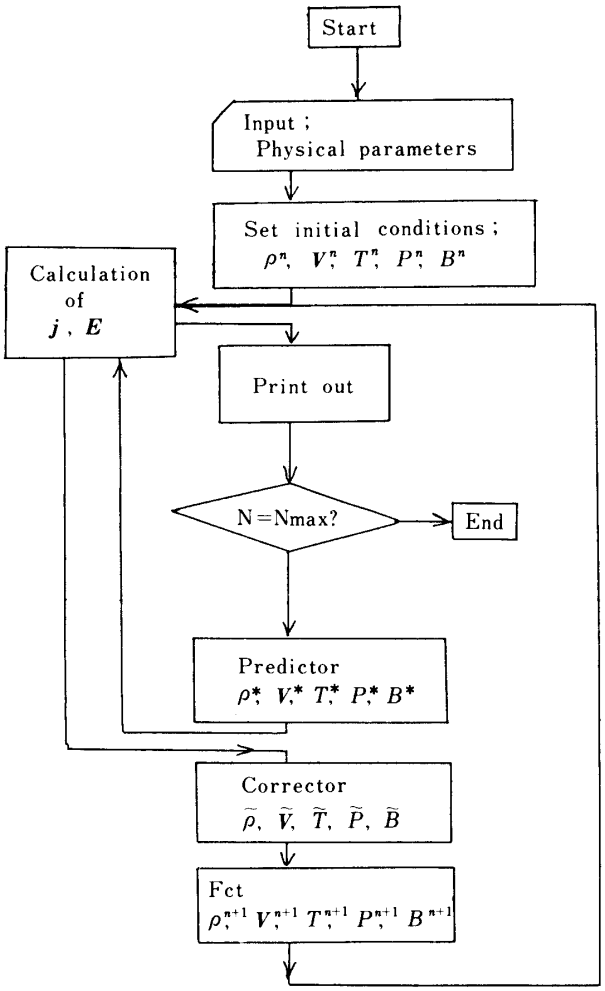

Fig. 3. Algorithm of numerical simulation.

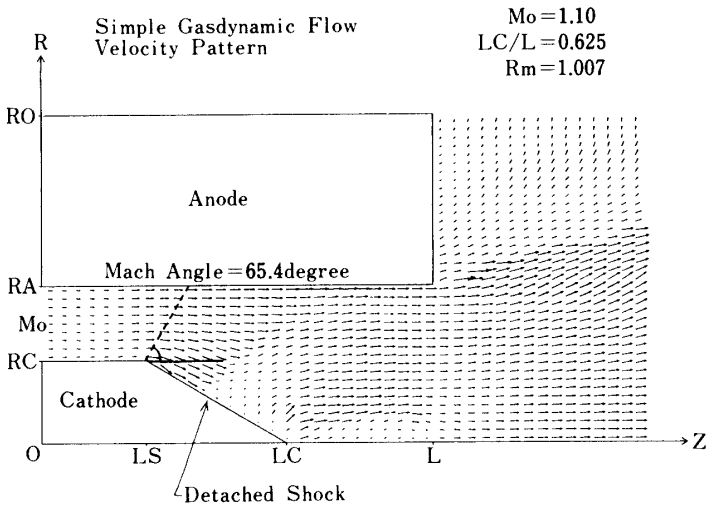

Fig. 4. Steady velocity distribution for a simple gasdynamic flow.

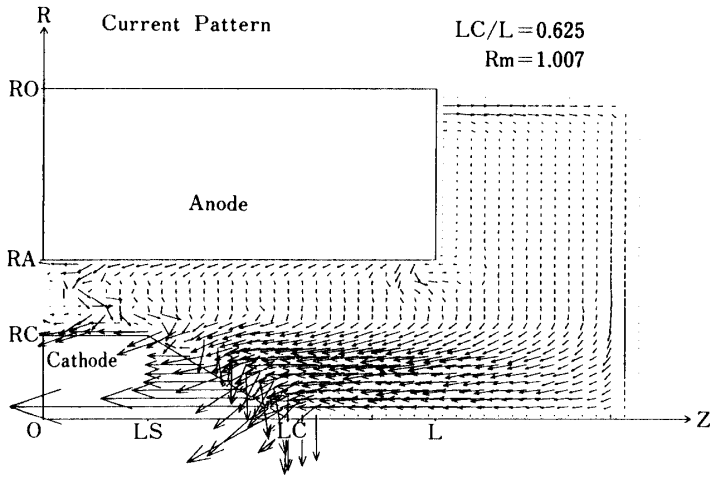

Fig. 5. Distribution of electric current density for $R_m=1.007$ and $L_c/L=0.625$, at time $t=36.6$ μsec.

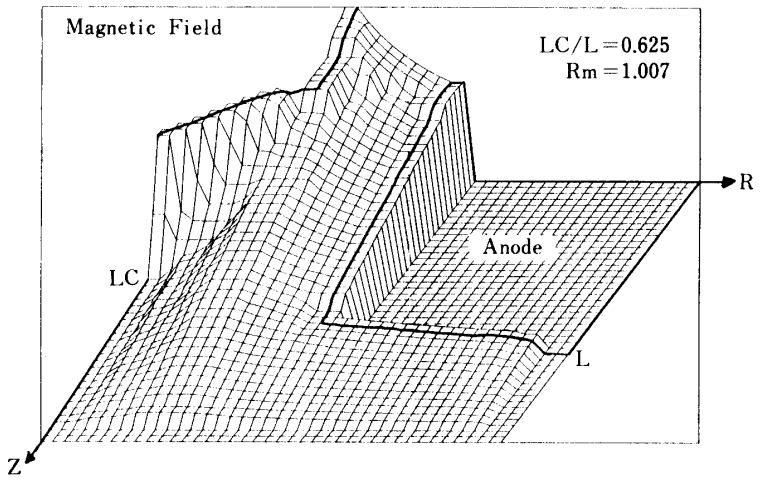

Fig. 6. Distribution of magnetic field for $R_m=1.007$ and $L_c/L=0.625$, at time $t=36.6$ μsec.

finite difference scheme with FCT technique. The algorithm of calculation is shown in Fig. 3.

Fig. 4 represents the velocity distribution for $B=0$, i.e., for a simple gasdynamic flow. Expansion occurs at the corner of the cathode while a detached shock wave is observed in the cathode tip region. The calculated Mach angle was 60 degrees, showing a reasonable agreement with the theoretical value 65.4 degrees corresponding to the incident Mach number $M=1.10$. As a result, it is confirmed that the present numerical code is trustworthy.

Figs. 5 and 6 show the distribution of electric current and magnetic field, both of which are still in a non-steady state even after 2200 steps. It is seen that the discharge current markedly flows into the cathode tip, with its direction nearly parallel to the z-axis in spite of the conical geometry. In the region of $R_c<r<R_0$, on the other hand, the current pattern is essentially radial except on the cathode and anode surfaces and on the calculation boundary $r=R$, where the current density is rather small. Magnetic field

distribution in Fig. 6 indicates that the magnetic field established on the cathode surface remains strong, particulary on the cathode tip.

REFERENCES

[*1*] Yoshikawa, T., Kagaya, Y. and Kuriki, K.: Thrust and Efficiency of New K-III MPD Thruster, AIAA Paper 82-1887 (1982).
[*2*] Spitzer, L. Jr.: Physics of Fully Ionized Gases, 2nd Revised Edition, Interscience Publishers (1962).
[*3*] Ao, T. and Fujiwara, T.: Numerical and Experimental Study of an MPD Thruster, 17th IEPC 84-08, pp. 56-64, JSASS/AIAA/DGLR (1984).